Journal of Alloys and Compounds, 206 (1994) 21–29
JALCOM 997

Solid state phase equilibria in the Ni–Ga–Sb system: experimental and calculated determinations

M.C. Le Clanche, S. Députier, J.C. Jégaden, R. Guérin
Laboratoire de Chimie du Solide et Inorganique Moléculaire, UA CNRS 1495, Université de Rennes I, Avenue du Général Leclerc, F-35042 Rennes Cédex (France)

Y. Ballini and A. Guivarc'h
FRANCE TELECOM, Centre National d'Etudes des Télécommunications, Lannion B (LAB/OCM/MPA), BP 40, F-22301 Lannion Cédex (France)

(Received September 16, 1993)

Abstract

Solid state phase equilibria in the ternary Ni–Ga–Sb diagram were established at 600 °C. The experimental techniques used to elaborate the phase equilibria were X-ray diffraction, electron probe microanalysis and scanning electron microscopy. A ternary phase with the nominal formula Ni_3GaSb (designated as A-phase in the present study) was evidenced. This phase exists over a broad range of homogeneity and exhibits hexagonal symmetry with a disordered structure derivative from NiAs and Ni_2In types. Very limited solid solubilities were measured in the constituent binary Ni–Ga and Ni–Sb compounds, with the exception of NiSb which showed a homogeneity range with a Ga-rich limit corresponding to the formula $Ni_2Ga_{0.25}Sb_{1.75}$. The phases GaSb, Ni_2Ga_3 and substituted-NiSb coexist with each other to form a three-phase equilibrium that dominates the GaSb side of the phase diagram. This part of the experimental diagram is in agreement with the calculated one from available experimental thermodynamic data on the Ga–Sb, Ni–Ga and Ni–Sb binaries and with interfacial reaction studies which concluded that Ni_2Ga_3 and substituted-NiSb are the stable phases when Ni thin films are reacted to completion on GaSb. A comparative study with the Ni–Ga–As and Ni–Al–As phase diagrams is also given which points out that, contrary to NiGa (NiAl) with GaAs (AlAs), the monogallide NiGa is not in thermodynamic equilibrium with GaSb.

1. Introduction

The development of metallic contacts to compound semiconductors which are stable at high temperatures, reliable and laterally uniform is an essential step in the ongoing miniaturization of electronic and opto-electronic devices [1–3].

The technological limitations of elemental contacts led to the empirical development of multi-elemental contacts, such as the Au–Ge–Ni ohmic metallization system for n-type III–V semiconductors (III–V SC). These metal/III–V SC systems with five or more components could only be understood if the simpler elemental metal/III–V semiconductors (M/III–V SC) were first explored in detail. Previous work has demonstrated the need for phase diagrams in rationalizing the reactions of metals with III–V SC and in researching stable contacts [4–6]. Indeed, the knowledge of which phases are in thermodynamic equilibrium with the III–V SC is therefore of practical importance. Unfortunately, such diagrams are not generally available, although great effort has been made recently to determine ternary M–III–V phase diagrams from bulk experiments [7–14]. Consequently, in most of the cases, the estimation of these diagrams is made either by using available experimental or calculated thermodynamic data [15, 16] for the three binary systems (M–III element, M–V element and III–V) or by deducing them from known ternary systems which may be *a priori* analogous.

This paper deals with the Ni–Ga–Sb system. First, an isothermal section of the bulk phase diagram has been experimentally determined at 600 °C. Then, a comparative study with the ternary phase diagram calculated from available experimental and estimated thermodynamic data on the binary compounds has been made in order to test, in a general manner, the validity of calculated diagrams. Finally, the isothermal section of the Ni–Ga–Sb phase diagram has been compared with the Ni–Ga–As [17–19] and the Ni–Al–As [20–22] ones that we previously studied. The results on the interfacial reactions of Ni thin films on (001) and (111)

SSDI 0925-8388(93)00997-D

GaSb, which are in agreement with the bulk phase diagram, will be published elsewhere [23].

2. Experimental determination of the Ni–Ga–Sb phase diagram

2.1. Experimental details

The samples were prepared by direct combination of the elements: the starting materials were powders (nickel and antimony) or ingots (gallium), all with minimum impurity 99.9%. The elements were intimately mixed (total sample about 800 mg) and placed in silica tubes which were evacuated to 10^{-3} Torr, sealed and placed in a resistance furnace. Samples were first annealed at 1000 °C for 24 h and subsequently cooled to 600 °C and annealed at that temperature over a period of 72 h. After cooling, the samples were ground to powder, cold pressed into pellets, sealed again and annealed at 600 °C for 10 days to ensure homogeneity. Finally, samples were quenched in ice water. In some cases, especially for Ni-rich samples, several grindings and re-annealings at 600 °C over a long period of time were needed to reach thermodynamic equilibrium.

The pellets were removed from the quartz ampoules and cut in half. One half of each sample was pulverized and analyzed using a powder diffractometer (CPS 120 Inel) equipped with a position-sensitive detector covering 120° in 2θ (elemental silica was taken to determine a cubic spline calibration function to describe the 2θ *vs.* channel number function). The second half was embedded in epoxy resin and polished down to 0.25 μm diamond grade. The sample was then coated with either a gold or graphite thin layer to obtain good surface conductivity. Composition analysis was done with a Camebax SX50 electron microprobe using wavelength-dispersive spectroscopy (WDS) of X-rays. GaSb and pure nickel in ingot form were used as standards. Backscattered electron imaging was done with a Jeol JSM-35C scanning electron microscope. The compositional data were carefully checked against the diffraction data to identify the phases present in each sample.

2.2. Experimental results

2.2.1. The constituent binaries

Prior to discussing the experimental data obtained in the present study for the ternary Ni–Ga–Sb system at 600 °C, let us first review the binary data reported in the literature [8, 17, 24–30]. The phases' stabilities and crystallographic data of intermediate binary phases are best known in the Ga–Sb system, followed by the Ni–Ga and Ni–Sb systems. The X-ray diffraction patterns of the binaries observed in this study at 600 °C were compared with those previously reported.

The only intermediate phase in the Ga–Sb system is GaSb; its structure, lattice parameter and melting point are taken from the literature as given in Table 1.

Previous investigations [24–28] and our own studies [17] revealed that several intermetallic phases occur in the Ni–Ga system: Ni_3Ga, Ni_5Ga_3, γNi_3Ga_2, $Ni_{13}Ga_9$, NiGa, Ni_3Ga_4, Ni_2Ga_3, $NiGa_4$. Among them, Ni_3Ga_4 and $NiGa_4$ are not observed at 600 °C. At 790±30 °C, the phase Ni_3Ga_2 undergoes a transition from the disordered form, γNi_3Ga_2, to a "superlattice" structure which was first considered to be $\gamma' Ni_3Ga_2$ [25], but was structurally recognized more recently as $Ni_{13}Ga_9$ [31]. It is also important to note that the maximal solubility of Ga in (Ni) is about 14 at.% at 600 °C and that the homogeneity range of Ni_3Ga extends from 23 at.% to 30 at.% Ga, while that of NiGa is between 47 and 55 at.% Ga. The structural data and temperature stabilities for all the binaries in the Ni–Ga system are summarized in Table 1.

The phase equilibrium data for the Ni–Sb system indicate that four intermediate phases occur at 600 °C: Ni_3Sb, Ni_5Sb_2, NiSb and $NiSb_2$ [27–30]. Contrary to Ni_3Sb, Ni_5Sb_2 and $NiSb_2$, the NiSb binary shows, at 600 °C, a homogeneity range which extends, in our study, from 47 to 53 at.% Ni, very close to the 46 to 54 at.% Ni given in the literature. The hexagonal unit cell constants decrease from $a_h = 0.3995(1)$ nm, $c_h = 0.5175(1)$ nm for $Ni_{47}Sb_{53}$ to $a_h = 0.3958(1)$ nm, $c_h = 0.5150(1)$ nm for $Ni_{53}Sb_{47}$, in agreement with the Sb content. Another phase, Ni_7Sb_3 (no available crystallographic data), is also mentioned in the literature, but has not been observed during the study at 600 °C, since Ni_7Sb_3 decomposes at 582 °C: $Ni_7Sb_3 + NiSb \leftrightarrow Ni_5Sb_2$. The solubility range of Sb in (Ni) has been reported to be 9%. The summary of the Ni–Sb binary phases is given in Table 1.

2.2.2. The ternary Ni–Ga–Sb system

According to the review given above, the stable binary phases at 600 °C are Ni_2Ga_3, NiGa, $Ni_{13}Ga_9$, Ni_5Ga_3, Ni_3Ga, Ni_3Sb, Ni_5Sb_2, NiSb, $NiSb_2$ and GaSb. On the basis of these binaries, the ternary Ni–Ga–Sb diagram has been built (pure gallium is the only liquid phase at the diagram temperature). A total of about 30 samples were prepared to establish the solid state phase equilibria of the Ni–Ga–Sb system at 600 °C (Fig. 1). The gross compositions of some samples (labelled 1–10), the phases identified by X-ray diffraction (XRD) and the compositions of the phases as determined by electron probe microanalysis (EPMA) are listed in Table 2.

Most of the binary phases in the system reveal small ternary solubilities, with the exception of NiSb which dissolves about 6 at.% Ga, leading to the Ga-rich limit $Ni_2Ga_{0.25}Sb_{1.75}$. The XRD pattern of NiSb and its Ga-

TABLE 1. Ni–Ga–Sb constituent binary phases, crystal structures, lattice parameters and temperature stabilities

Phases	Type structure, Pearson symbol	Lattice parameters (nm)	Temperature stability (°C)	References
GaSb	ZnS, cF8	$a=0.6100(1)$	706 (c)	27,28
Ni_3Ga	Cu_3Au, cP4	$a=0.3585(1)$	1212 (p)	17, 24–28
Ni_5Ga_3	Pt_5Ga_3, oC16	$a=0.7510(4)$; $b=0.6708(3)$; $c=0.3753(1)$	741 (pd)	24–28
$Ni_3Ga_2(\gamma)$	NiAs, hP4	$a=0.3995(3)$; $c=0.4980(4)$	$790<T<949$	24–28
$Ni_{13}Ga_9(\gamma')$	$Pt_{13}In_9$, mC44	$a=1.3822$; $b=0.7894$; $c=0.8478$; $\beta=35.88°$	$T<790$	27–28, 31
NiGa	CsCl, cP2	$a=0.2886(1)$	1220 (c)	17, 24–28
Ni_3Ga_4	Ni_3Ga_4, cI112	$a=1.1411(2)$	542 (pd)	17, 24–28
Ni_2Ga_3	Ni_2Al_3, hP5	$a=0.4054(1)$; $c=0.4882(2)$	895 (p)	24–28
$NiGa_4$	Cu_5Zn_8, cI52	$a=0.8424(3)$	363 (p)	24–28
Ni_3Sb[a]	βCu_3Ti, oP8	$a=0.5318(1)$; $b=0.4284(1)$; $c=0.4519(1)$	715 (p)	27–30
Ni_5Sb_2	Ni_5Sb_2, mC28	$a=1.2946$; $b=0.5427$; $c=1.1457$; $\beta=151.71°$	1161 (c)	27–30
NiSb[a]	NiAs, hP4	$a=0.3935(1)$; $c=0.5152(2)$	1147 (c)	27–30
$NiSb_2$[a]	FeS_2, oP6	$a=0.5183(2)$; $b=0.6313(3)$; $c=0.3836(1)$	616 (p)	27–30
Sb	αAs, hR2	$a=0.43084$; $c=1.1274$	630.5 (c)	27, 28
Ga	αGa, oC8	$a=0.4524$; $b=0.4523$; $c=0.7661$	29.77 (c)	27, 28

The symbol c denotes congruent melting; p denotes peritectic melting; pd denotes peritectoid decomposition.
[a]Unit-cell parameters which have been refined in this work.

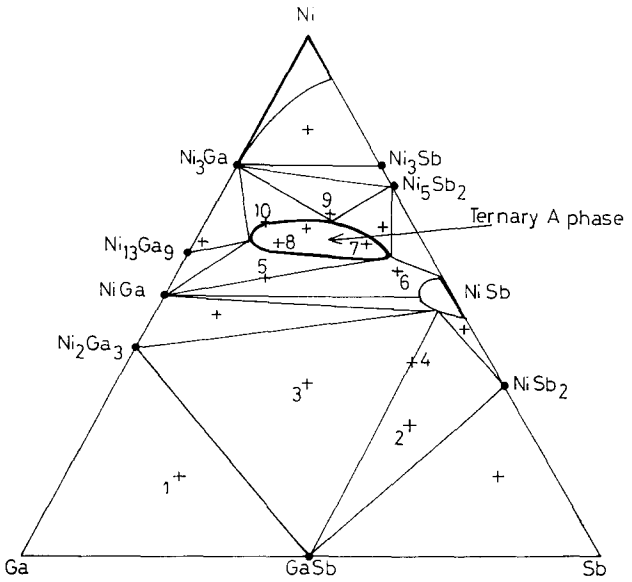

Fig. 1. Isothermal section of the Ni–Ga–Sb ternary diagram at 600 °C. Axes are in at.%. Compositions of the samples 1–10, reported in Table 2, are indicated.

TABLE 2. Gross sample compositions and phases identified by X-ray diffraction and EPMA for 600 °C isotherm

Sample number	Gross composition Ni:Ga:Sb (at.%)	Phases identified by X-ray diffraction	Composition of phases by EPMA Ni:Ga:Sb (at.%)
1	15:65:20	Ni_2Ga_3	40.2:59.8:0.1
		Ga	–
		GaSb	0.5:48.8:50.7
2	25:20:55	GaSb	–:49.1:50.9
		NiSb	47.3:2.1:50.6
		$NiSb_2$	33.2:0.5:66.3
3	33:33:33	Ni_2Ga_3	40.1:59.2:0.7
		GaSb	0.3:48.2:50.5
		NiSb	47.4:2.3:50.0
4	38:14:48	GaSb	0.3:47.2:52.5
		NiSb	47:6:2.1:50.3
5	53:31:16	NiGa	51.6:47.8:0.7
		A-phase	57.1:29.5:13.4
6	55:5:40	A-phase	57.9:6.6:35.5
		NiSb	54.2:3.3:42.5
7	60:10:30	A-phase	61.1:6.7:32.2
8	60:25:15	A-phase	62.9:21:16.1
9	64:15:21	A-phase	63.9:13.1:23.0
		Ni_3Ga	–
		Ni_5Sb_2	–
10	64:25:11	A-phase	65.4:21.7:12.9

rich limit are shown in Figs. 2(a) and (b), and their unit cell parameters are given in Table 3. The small solubilities in the other binaries were established mainly on the basis of EPMA analysis of equilibrated heterogeneous samples of overall compositions as indicated in Fig. 1 and Table 2.

The main feature of this isothermal section is the existence of a ternary phase with nominal formula Ni_3GaSb (this phase will also be designated the A-phase for further comparative study) in the Ni-rich part of the diagram. This ternary phase exists over a considerable range of composition, since it extends from approximately 60 at.% Ni, 10 at.% Sb, 30 at.% Ga (Ga-rich limit) to 55 at.% Ni, 38 at.% Sb, 7 at.% Ga (Sb-rich limit). Moreover, the upper and lower nickel

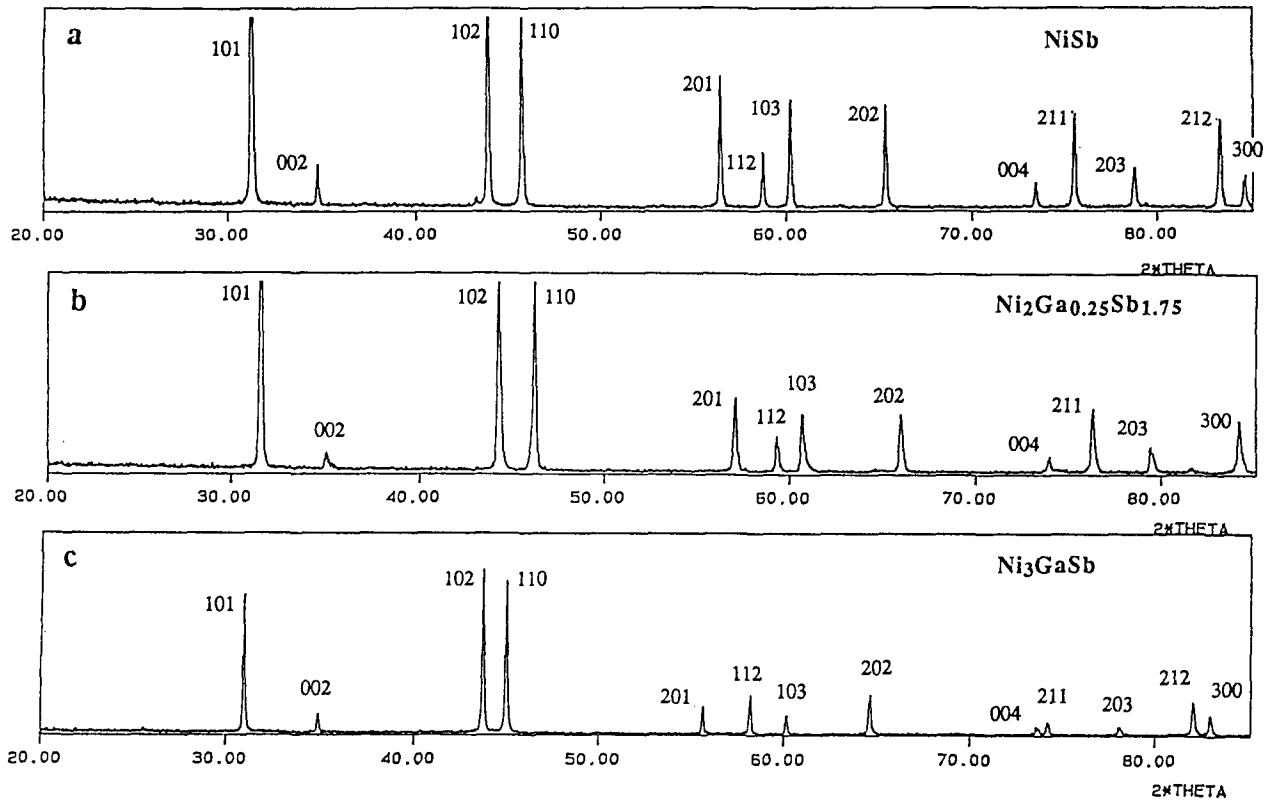

Fig. 2. X-ray diffraction pattern for (a) the binary NiSb, (b) its Ga-rich limit $Ni_2Ga_{0.25}Sb_{1.75}$ and (c) the ternary phase Ni_3GaSb (A-phase), ($\lambda_{Cu} = 1.540\,56$ Å).

TABLE 3. Crystallographic data for different atomic compositions of ternary A-phase and pseudo-binary NiSb phase

Composition (at.%)	Formula	a_h (nm)	c_h (nm)	V ($nm^3 \times 10^3$)	c/a
$Ni_{60}Ga_{20}Sb_{20}$	Ni_3GaSb	0.4028(1)	0.5141(2)	72.3	1.276
	Ni_3GaSb[a]	0.400	0.509	70.5	1.273
$Ni_{60}Ga_{30}Sb_{10}$	$Ni_3Ga_{1.5}Sb_{0.5}$	0.3990(1)	0.5042(2)	69.5	1.264
$Ni_{55}Ga_{20}Sb_{25}$	$Ni_{2.45}Ga_{0.90}Sb_{1.10}$	0.3973(1)	0.5097(1)	69.7	1.283
$Ni_{55}Ga_7Sb_{38}$	$Ni_{2.45}Ga_{0.30}Sb_{1.70}$	0.3989(1)	0.5153(1)	71.0	1.292
$Ni_{50}Sb_{50}$	NiSb	0.3946(1)	0.5148(1)	69.4	1.305
	NiSb[a]	0.394	0.516	69.4	1.310
$Ni_{50}Ga_6Sb_{44}$	$Ni_2Ga_{0.25}Sb_{1.75}$	0.3935(1)	0.5130(1)	68.80	1.304

[a]Lattice constants taken from ref. 33.

atomic concentrations for equi-atomic content in Sb and Ga correspond to $Ni_{3.40}GaSb$ (63 at.% Ni) and $Ni_{2.45}GaSb$ (55 at.% Ni), respectively. The XRD pattern and a scanning electron backscatter micrograph of the A-phase (nominal composition Ni_3GaSb) are shown in Figs. 2(c) and 3(a).

Another important result of the isothermal section of the ternary Ni–Ga–Sb phase diagram is the fact that, in addition to the ternary phase, a tie-line links NiSb (in fact $Ni_2Ga_{0.25}Sb_{1.75}$) to Ni_2Ga_3, preventing NiGa from being in thermodynamic equilibrium with GaSb. Therefore a three-phase region GaSb, Ni_2Ga_3 and NiSb dominates the GaSb side of the phase diagram; no NiGa–GaSb tie-line is observed, contrary to what happens in the Ni–Ga–As system, where a NiGa–GaAs tie-line occurs [17] (see Section 4). A micrograph of sample 3 exhibiting the microstructure of the NiSb, Ni_2Ga_3 and GaSb mixture is shown in Fig. 3(b). Another three-phase equilibrium GaSb + NiSb + $NiSb_2$ was confirmed by sample 2, which was located in this region. It is important to remember that all of these data are of great importance for developing metallization schemes of GaSb using nickel as a contact element.

In the Ni-rich region of the diagram, numerous tie-lines connecting binaries and the ternary A-phase have been deduced from XRD and EPMA experiments.

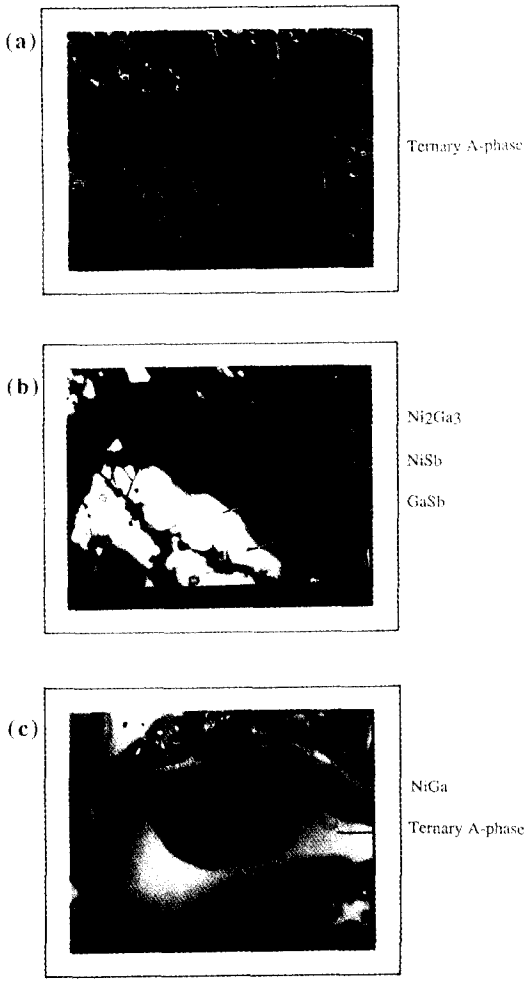

Fig. 3. Scanning electron backscatter micrographs showing (a) single-phase structure Ni_3GaSb, (b) three-phase mixture: NiSb, Ni_2Ga_3, GaSb (sample 3) and (c) two-phase mixture: NiGa and A-phase (sample 5).

Figure 3(c) shows a micrograph of sample 5 exhibiting a two-phase structure, which clearly denotes the presence of NiGa and the ternary A-phase. The miscibility gap between the A-phase and NiSb, both phases exhibiting hexagonal symmetry, and the same NiAs-type structure (see Section 4) has been established by EPMA experiments on the basis of sample 6, grains of the microstructure showing unambiguously two different values in atomic composition (Table 2).

In the classification of ternary phase diagrams described by Beyers *et al.* [6], the Ni–Ga–Sb system could be seen as belonging to type V, since a ternary phase exists. Nevertheless this phase is not in thermodynamic equilibrium with GaSb; therefore all of the general features of the diagram correspond essentially to type IV.

2.2.3. *The ternary A-phase*

This phase, the homogeneity range of which has been defined above, crystallizes in hexagonal symmetry and exhibits a crystal structure which is an intermediate of the $B8_1$(NiAs) and $B8_2$(Ni_2In) structures (Fig. 4). In this structure, the additional nickel is randomly distributed on one of the two equivalent interstitial sites, since the structure is disordered. In the $B8_2$ structure, both of these sites are occupied by atoms, whereas in the $B8_1$ structure they are both vacant. Therefore the ternary phase appears either as a partly filled NiAs-type or as a defective Ni_2In-type structure ($B8_{1.5}$). Moreover, it can be seen that Sb and Ga atoms are also randomly distributed in the non-metal sublattice, since no extra reflections in XRD powder patterns inducing a superstructure have been observed (Fig. 2). In addition, Table 3 shows that lattice constants for different atomic compositions of the A-phase vary *vs.* nickel content and Sb–Ga substitution, in agreement with the covalent radius (1.40 Å for Sb instead of 1.26 Å for Ga) [32]. It can be seen that the ternary A-phase has recently been reported in the literature [33]. The results of DTA experiments indicated that Ni_3GaSb melts at 1066 °C. The authors suggested that the ternary phase was not really a ternary compound, but rather represented specific compositions of an extensive solid solution starting from NiSb up to Ni_3Ga_2, since the first one is of NiAs-type ($B8_1$) and the second one of defective Ni_2In-type ($B8_{1.5}$). At first glance, the broad homogeneity range and the shape we have found here for the A-phase seems to corroborate this assumption. However, the stability range of Ni_3Ga_2 (790 °C $< T <$ 940 °C) shows that such a continuous solid solution does not exist at 600 °C; on the other hand, our own results suggest that a miscibility gap occurs between NiSb and the ternary A-phase. Moreover, the hypothesis of an extensive solid solution could also be expressed for the ternary Ni–Ga–As phase diagram; in fact, five successive phases between NiAs and Ni_3Ga_2 were synthesized from bulk experiments [17] (see Section 4). It can be

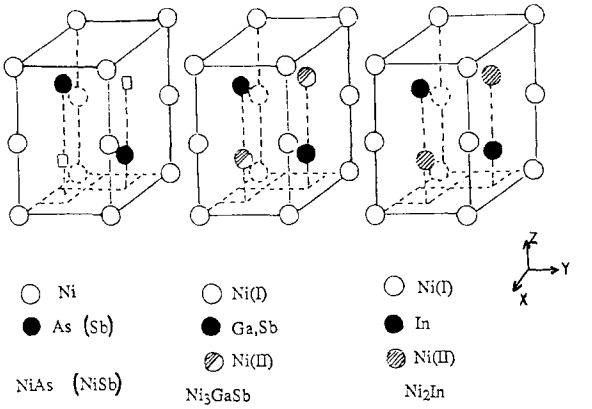

Fig. 4. Representation of the structures NiAs($B8_1$), Ni_3GaSb($B8_{1.5}$) and Ni_2In($B8_2$). Ni and non-metal atoms are respectively schematized by white and black circles; extra Ni atoms in half (Ni_3GaSb) or full (Ni_2In) occupancy are represented by streaked circles.

noted that immiscibility problems are at the present time fully analysed theoretically and that their thermodynamic analysis is made on the basis of free calculations expressed in terms of crystal lattice distortion energies as a function of the solid solution composition. Such a situation was, for example, observed in the study of the solid solution Rh_2As–Rh_2P of anti-fluorine type structure [34].

3. The calculated Ni–Ga–Sb phase diagrams

If thermodynamic data on all the pertinent binary phases are available, the M–III–V phase diagrams can be calculated. It is interesting to test the validity of such approaches, because many ternary phase diagrams have not been determined experimentally up to now. For this purpose, the Ni–Ga–Sb system is well suited,

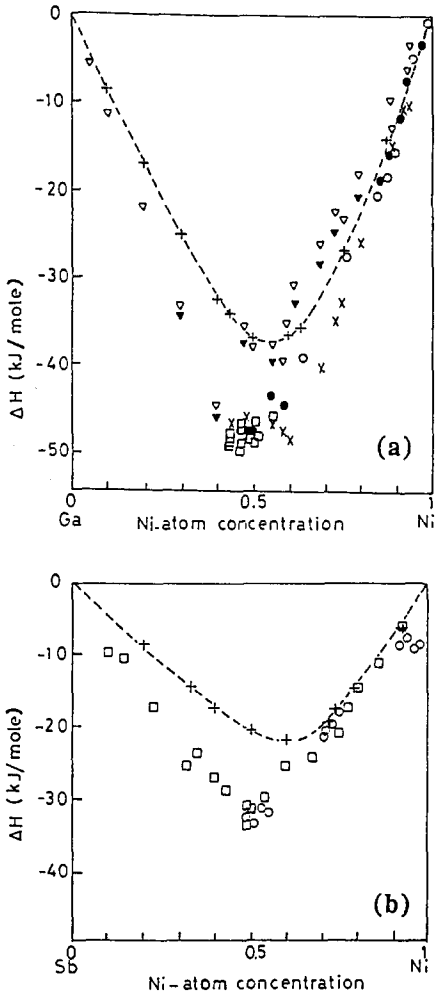

Fig. 5. Experimental formation enthalpies of binaries in the (a) Ni–Ga and (b) Ni–Sb systems. Different marks correspond to the experimental values given in refs. 36–41. The dashed lines correspond to the enthalpies theoretically estimated from the "semi-empirical" Miedema's model [42–46].

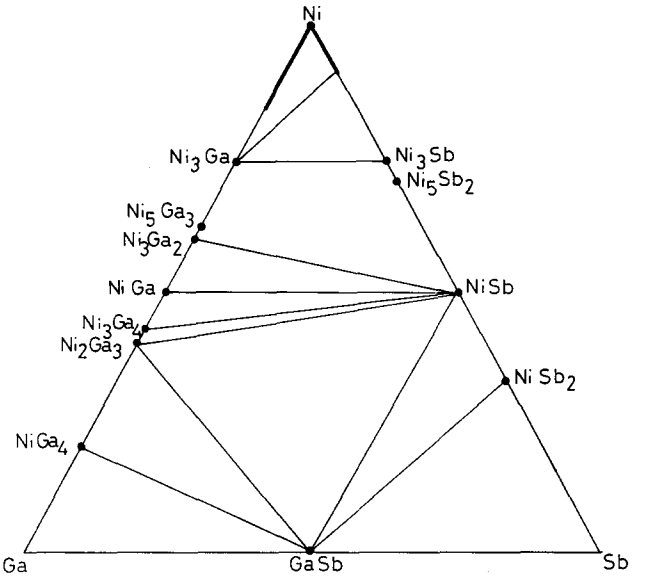

Fig. 6. Ni–Ga–Sb ternary diagram calculated from experimental formation enthalpies.

owing to the occurrence of available and numerous experimental thermodynamic data for all the binary systems: Ga–Sb, Ni–Ga and Ni–Sb [35–41].

In order to perform predictions of the ternary diagrams, Schmidt-Fetzer [15] proposed using the following simplifications:

1. No ternary M–III–V exists.
2. The binary phases are represented as points in an isothermal section of the phase diagram, *i.e.* the solid solubilities are disregarded.
3. The Gibbs energy of formation of the various solid phases ($\Delta G°$) is approximated by the formation enthalpy ($\Delta H°$).

If this last assumption is not too important here, the first two are very severe and clearly not suitable in the case of the Ni–Ga–Sb system.

The experimental formation enthalpies of the Ni–Ga and Ni–Sb binaries are shown in Figs. 5(a) and (b). Keeping the values for GaSb published by Schottky [35], the calculations lead to the diagram shown in Fig. 6 (the dispersion in the experimental values of enthalpies does not significantly affect the diagram). This diagram obviously differs from the experimental one (Fig. 1) in the Ni-rich part, which is dominated by the ternary A-phase. However, both diagrams are similar on the GaSb side, since a three-phase region Ni_2Ga_3–NiSb–GaSb is identically observed, which means that Ni_2Ga_3 and NiSb are the compounds in equilibrium with GaSb.

When the experimental thermodynamic data are lacking for binary compounds, the standard enthalpies of formation can be theoretically estimated from the "semi-empirical" Miedema's model [42–46]. This model has been conceived for metallic binary compounds with at least one transition metal as constituent. Miedema's

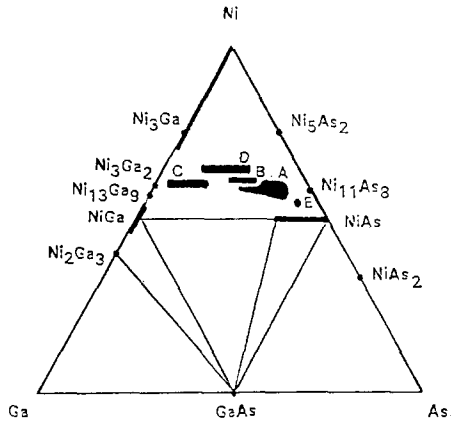

(a) Ni-Ga-As

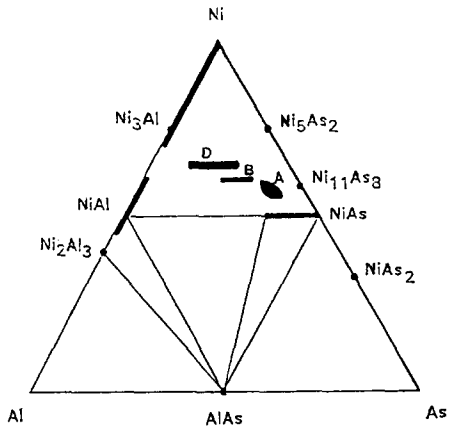

(b) Ni-Al-As

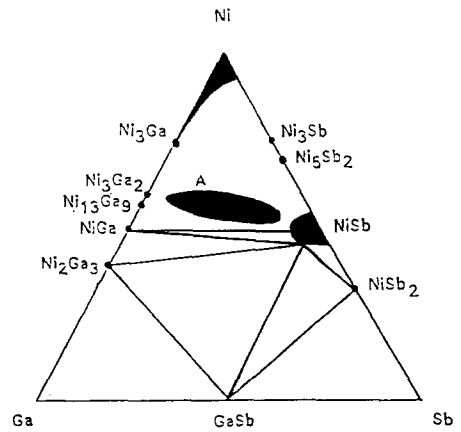

(c) Ni-Ga-Sb

Fig. 7. Isotherm sections of the (a) Ni–Ga–As (800 °C), (b) Ni–Al–As (800 °C) and (c) Ni–Ga–Sb (600 °C) phase diagrams. For simplification, only the ternary phases have been located in the Ni-rich part of the diagrams. The tie-lines, which are of great importance for determining potential binary candidates in metallization contacts on III–V semiconductors, are drawn in the bottom part.

calculated values of formation enthalpies can be compared with the experimental ones in Figs. 6(a) and (b) (dashed lines). It can be noted that the formation enthalpies are undervalued for less Ni-rich binaries. In his comments, Miedema effectively noticed a peculiar behaviour of the Ni, Pd and Pt metals that requires a corrective term in the calculations when the Ni, Pd or Pt concentration is lower than 50% in the compound. Therefore the theoretical Ni–Ga–Sb ternary diagram (not reported) differs significantly from the experimental one, showing in particular a wrong three-phase region NiSb–NiGa–GaSb involving a NiGa–GaSb tie-line instead of the true Ni_2Ga_3–NiSb one. This result points out the limits of the theoretical calculations based on Miedema's model to determine the ternary phase diagrams.

4. Comparative study with ternary phase diagrams Ni–Ga–As and Ni–Al–As

We reported previously solid state phase equilibria at 800 °C in both ternary Ni–Ga–As and Ni–Al–As systems [17, 20–22].

The ternary phase diagrams are given in Fig. 7. Five ternary phases which crystallize in hexagonal symmetry and may be structurally derived from the NiAs type were evidenced in the upper part of the Ni–Ga–As phase diagram [17] (Fig. 7(a)). These phases, most of them with broad homogeneity ranges, were labelled as phases A, B, C, D and E. Among them, three phases B, C and E showed hexagonal superlattices, with lattice constants $a\sqrt{3}\times 3c$, $2a\times 4c$ and $3a\times 2c$ respectively, which denoted ordered structures, while phases A and D were found to be wholly disordered (a, c). In the case of the ternary Ni–Al–As phase diagram [20–22], three phases with broad homogeneity range and isostructural to A, B and D phases were also found (Fig. 7(b)). The Ni–Ga–Sb diagram appears easier, since only one ternary phase, labelled as A-phase for comparison, has been found but with a largest homogeneity range (Fig. 7(c)). This result is probably due to the larger covalent radius of Sb (1.44 Å) compared with that of As (1.18 Å) [32] which allows the non-metal sublattice to accept additional nickel atoms without ordered structure rearrangement. The main feature of these ternary systems is that neither nickel nor ternary phases are in thermodynamic equilibrium with GaAs or AlAs or GaSb.

In the bottom part of the ternary phase diagrams, the binaries NiGa (or NiAl), Ni_2Ga_3 (or Ni_2Al_3) and NiAs were found to be in equilibrium with GaAs (or AlAs) for the Ni–Ga–As (or Ni–Al–As) systems (Figs. 7(a) and (b)) while in the case of Ni–Ga–Sb the existence of a three-phase region Ni_2Ga_3, NiSb and GaSb excludes

the binary NiGa to be connected by a tie-line to GaSb (Fig. 7(c)). This result is of great importance for developing metallization nickel contacts on such III–V binaries. Since the use of ternary phase diagrams enables one to rationalize the sequence of reaction products at Ni/III–V SC interfaces and considering that the average composition of a reacted Ni thin film with the III–V SC remains on the vertical line connecting Ni and the III–V binary, these results show unambiguously that NiGa (or NiAl) and NiAs must be the final phases of the interfacial Ni/GaAs (or Ni/AlAs) reaction and that Ni_2Ga_3 and NiSb are those of the Ni/GaSb one. However, the experimental diagrams predict that several Ni-rich phases, including ternary phase compositions in regions of three- or two-phase equilibrium, may precede the formation of final equilibrium products. Effectively, all of these assumptions were confirmed during the various steps of the solid state interdiffusions Ni/GaAs, Ni/AlAs and Ni/GaSb [18–23]. Moreover, these studies pointed out that NiGa and NiAl, highly textured in the final thin film reactions, must be considered as good candidates for the thermodynamically stable contacts to GaAs and AlAs respectively. As a consequence, epitactic matched NiGa/GaAs, NiAl/AlAs, GaAs/NiGa/GaAs and AlAs/NiAl/AlAs have recently been realized [47–50]. It is worth noting that the hexagonal pseudo-cubic structure of Ni_2Ga_3 and its large mismatch with the substrate ($\delta a/a \approx 8\%$) do not permit the consideration of Ni_2Ga_3 as a potential candidate for stable and epitactic contacts on GaSb (001) 23).

5. Conclusion

In this study the isothermal phase diagram for Ni–Ga–Sb was determined at 600 °C. Limited solubility was measured in each of the constituent binary phases, with the exception of NiSb which dissolves 6 at.% Ga (nominal composition $Ni_2Ga_{0.25}Sb_{1.75}$). The existence of a ternary phase with a broad homogeneity range and located in the upper part of the diagram was pointed out. This A-phase crystallizes in hexagonal symmetry and may be structurally derived from the NiAs-type structure. The occurrence of a GaSb–Ni_2Ga_3–NiSb three-phase equilibrium triangle, suggested by calculations based on the experimental formation enthalpies of Ni–Ga, Ni–Sb and Ga–Sb binaries was experimentally confirmed. At last, a comparative study of the three quite equivalent diagrams Ni–Ga–As, Ni–Al–As and Ni–Ga–Sb pointed out important differences which justify that no general conclusions can be deduced from *a priori* equivalent ternary phase diagrams. Therefore the knowledge of each experimental phase diagram is absolutely necessary to understand and describe clearly the successive sequences of phase formation when metal/SC contacts are annealed.

Acknowledgements

This work was supported by the Centre National d'Etudes des Télécommunications, CNET Lannion B (FRANCE TELECOM) under contract 91 8B 062. One of us (MCLC) acknowledges the Conseil Régional de Bretagne for a research grant.

References

1 A. Piotrowska, A. Guivarc'h and G. Pelous, *Solid State Electron., 26* (1983) 179.
2 C.J. Palmstrøm and D.V. Morgan, in M.J. Howes and D.V. Morgan (eds.), *Gallium Arsenide Materials, Devices and Circuits,* Wiley, NY, 1985, p. 195.
3 T. Sands, *Mater. Sci. Eng. B, 1* (1989) 289.
4 R.S. Williams, J.R. Lince, C.T. Tsai and J.H. Pugh, *MRS Symposia Proc., 54,* Materials Research Society, Pittsburgh, PA, 1986, p. 335.
5 T. Sands, *J. Met., 38* (1986) 31.
6 R. Beyers, K.B. Kim and R. Sinclair, *J. Appl. Phys., 61* (1987) 2195.
7 M. El Boragy and K. Schubert, *Z. Metallkd., 72* (1981) 279.
8 X.Y. Zheng, J.C. Lin, D. Swenson, K.C. Hsieh and Y.A. Chang, *Mater. Sci. Eng. B, 5* (1989) 63.
9 K.J. Schulz, X.Y. Zheng and Y.A. Chang, *Bull. Alloy Phase Diag., 10* (1989) 314.
10 F.Y. Shiau, Y. Zuo, J.C. Lin, X.Y. Zheng and Y.A. Chang, *Z. Metallkd., 80* (1989) 544.
11 X.Y. Zheng, K.J. Schultz, J.C. Lin and Y.A. Chang, *J. Less-Common Met., 146* (1989) 233.
12 R. Guérin, A. Guivarc'h, Y. Ballini and M. Secoué, *Rev. Phys. Appl., 25* (1990) 411.
13 K.J. Schultz, O.A. Musbah and Y.A. Chang, *J. Phase Equilibria, 12* (1991) 10.
14 S. Députier, R. Guérin, Y. Ballini and A. Guivarc'h, *J. Alloys Comp., 202* (1993) 95.
15 R. Schmid-Fetzer, *J. Elect. Mat., 17* (1987) 193.
16 N.A. Testova, A.N. Golubenko, G.A. Kokovin and S.V. Sysoev, *Izv. Akad. Nauk SSSR, Neorg. Mater., 22* (1986) 1781.
17 R. Guérin and A. Guivarc'h, *J. Appl. Phys., 66* (1989) 2122.
18 A. Guivarc'h, R. Guérin, J. Caulet, A. Poudoulec and J. Fontenille, *J. Appl. Phys., 66* (1989) 2129.
19 A. Poudoulec, B. Guenais, A. Guivarc'h, J. Caulet and R. Guérin, *J. Appl. Phys., 70* (1991) 7613.
20 R. Guérin, S. Députier, J. Caulet, M. Minier, A. Poudoulec, Y. Ballini, V. Durel, G. Dupas and A. Guivarc'h, *MRS Symposia Proc., 160,* Materials Research Society, Pittsburgh, PA, 1990, p. 319.
21 S. Députier, *Thèse d'Université,* Rennes, 1992.
22 S. Députier, R. Guérin, J. Caulet, M. Minier, Y. Ballini and A. Guivarc'h, *J. Phys. III,* in press.
23 A. Guivarc'h, J. Caulet, M. Minier, M.C. Le Clanche, S. Députier and R. Guérin, *J. Appl. Phys.,* in press.
24 E. Hellner and F. Laves, *Z. für Naturf., 2a* (1947) 177.
25 E. Hellner, *Z. Metallkd., 41* (1950) 480.

26 P. Feschotte and P. Eggimann, *J. Less-Common Met., 63* (1979) 15.
27 T.B. Massalski, in *Binary Alloy Phase Diagrams,* 2nd edn., American Society for Metals, Metals Park, OH, 1990.
28 P. Villars and L.D. Calvert, in *Pearson's Handbook of Crystallographic Data for Intermetallic Phases,* American Society for Metals, Metals Park, OH, 1991.
29 J. Naud and D. Parijs, *Mater. Res. Bull., 7* (1972) 301.
30 P. Feschotte and D. Lorin, *J. Less-Common Met., 155* (1989) 255.
31 M. Ellner, S. Bhan and K. Schubert, *J. Less-Common Met., 19* (1969) 245.
32 L. Pauling, in *Nature of the Chemical Bond,* 3rd edn., Cornell University Press, Ithaca, NY, 1960.
33 C.H. Jan and Y.A. Chang, *J. Mater. Res., 6* (1991) 2660.
34 M. Secoué, P. Auvray, Y. Toudic, Y. Ballini and R. Guérin, *J. Cryst. Growth, 76* (1986) 131.
35 W.F. Schottky and M.B. Bever, *Acta Met., 6* (1958) 320.
36 H. Jacobi, D. Stöckel and H.L. Lukas, *Z. Metallkd., 62* (1971) 305.
37 J.N. Pratt, J.M. Bird and S. Martosudirjo, *Technical Report Data 37-72-C-3034* (1973).
38 S. Martosudirjo and J.N. Pratt, *Thermochim. Acta, 17* (1976) 183.
39 B. Predel, W. Vogelbein and U. Schallner, *Thermochim. Acta, 12* (1975) 367.
40 F. Körber and W. Oelsen, *Mitt. Kaiser Wilhelm Inst. Eisenforschung Düsseldorf, 19* (1937) 209.
41 B. Predel and W. Vogelbein, *Thermochim. Acta, 24* (1978) 155.
42 A.R. Miedema, R. Boom and F.R. de Boer, *J. Less-Common Met., 41* (1975) 283.
43 A.R. Miedema, *J. Less-Common Met., 46* (1976) 67.
44 A.R. Miedema, P.F. de Châtel and F.R. de Boer, *Physica B, 100* (1980) 1.
45 A.K. Niessen, F.R. de Boer, R. Boom, P.F. de Châtel, M.C.M. Mattens and A.R. Miedema, *Calphad, 7* (1983) 51.
46 F.R. de Boer, R. Boom, M.C.M. Mattens, A.R. Miedema and A.K. Niessen, *Cohesion in Metals–Transition Metal Alloys,* North Holland, Amsterdam, 1988.
47 A. Guivarc'h, R. Guérin and M. Secoué, *Electron. Lett., 23* (1987) 1004.
48 V. Durel, *Thèse d'Université,* Rennes, 1991.
49 V. Durel, B. Guenais, Y. Ballini, J. Caulet, M. Minier and A. Guivarc'h, *Inst. Phys. Conf. Ser., 112* (1991) 129.
50 C.J. Palmstrøm and T. Sands, in L.J. Brillson (ed.), *Contacts to Semiconductors,* Noyes, Park Bridge, NJ, 1993, in press.